Author/s:
Gransbury, GK;Livesay, BN;Janetzki, JT;Hay, MA;Gable, RW;Shores, MP;Starikova, A;Boskovic, C

Title:
Understanding the Origin of One- or Two-Step Valence Tautomeric Transitions in Bis(dioxolene)-Bridged Dinuclear Cobalt Complexes

Date:
2020-06-17

Citation:
Gransbury, G. K., Livesay, B. N., Janetzki, J. T., Hay, M. A., Gable, R. W., Shores, M. P., Starikova, A. & Boskovic, C. (2020). Understanding the Origin of One- or Two-Step Valence Tautomeric Transitions in Bis(dioxolene)-Bridged Dinuclear Cobalt Complexes. Journal of the American Chemical Society, 142 (24), pp.10692-10704. https://doi.org/10.1021/jacs.0c01073.

Understanding the Origin of One- or Two-Step Valence Tautomeric Transitions in Bis(dioxolene)-Bridged Dinuclear Cobalt Complexes

Gemma K. Gransbury,[†] Brooke N. Livesay,[‡] Jett T. Janetzki,[†] Moya A. Hay,[†] Robert W. Gable,[†] Matthew P. Shores,[‡] Alyona Starikova,[§] Colette Boskovic[,†]*

[†] School of Chemistry, University of Melbourne, Parkville, VIC 3010, Australia

[‡] Department of Chemistry, Colorado State University, Fort Collins 80523, USA

[§] Institute of Physical and Organic Chemistry, Southern Federal University, 344090 Rostov-on-Don, Russian Federation

ABSTRACT

Valence tautomerism (VT) involves a reversible stimulated intramolecular electron transfer between a redox-active ligand and redox-active metal. Bis(dioxolene)-bridged dinuclear cobalt compounds provide an avenue toward controlled two-step VT interconversions of the form {Co^{III}-cat-cat-Co^{III}} ⇌ {Co^{III}-cat-SQ-Co^{II}} ⇌ {Co^{II}-SQ-SQ-Co^{II}} (cat^{2-} = catecholate, $SQ^{\bullet-}$ = semiquinonate). Design flexibility for dinuclear VT complexes confers an advantage over two-step spin crossover complexes for future applications in devices or materials. The four dinuclear cobalt complexes in this study are bridged by deprotonated 3,3,3′,3′-tetramethyl-1,1′-spirobi(indan)-5,5′,6,6′-tetraol (spiroH_4) or 3,3,3′,3′-tetramethyl-1,1′-spirobi(indan)-4,4′,7,7′-tetrabromo-5,5′,6,6′-tetraol (Br_4spiroH_4) with Me_ntpa ancillary ligands (tpa = tris(2-pyridylmethyl)amine, n = 0–3 corresponds to methylations of the 6-position of the pyridine rings). Complementary structural, magnetic, spectroscopic and DFT computational studies reveal different electronic structures and VT behavior for the four cobalt complexes; one-step one-electron partial VT, two-step VT, incomplete VT, and temperature-invariant {Co^{III}-cat-cat-Co^{III}} states are observed. Electrochemistry, DFT calculations and the study of a mixed-valence {Zn^{II}-cat-SQ-Zn^{II}} analog have allowed elucidation of thermodynamic parameters governing the one- and two-step VT behavior. The VT transition profile is rationalized by 1) the degree of electronic communication within the bis(dioxolene) ligand and 2) the matching of cobalt and dioxolene redox potentials. This work establishes a clear path to the next generation of two-step VT complexes through incorporation of mixed-valence class II and class II-III bis(dioxolene) ligands with sufficiently weak intramolecular coupling.

INTRODUCTION

Molecular materials that can be switched between two or more physically distinguishable states by external stimuli have far-reaching future prospects in materials with applications ranging from sensing and display devices to quantum computing, molecular electronics and molecular spintronics.[1-3] Physical distinction of states enables colorimetric readout as a diode, sensor or display, and is implemented in devices by attaching molecules to surfaces or incorporating them into thin films.[2-5] Recently, switchable molecules have been used to selectively address spins for initialization, manipulation and readout in quantum information processing.[6-7] Multifunctional molecules are also under consideration for spin-switching and spin-filtering applications in spintronics, and could be used for data storage as a molecular metal spin can be manipulated and readout at the nanoscale.[1,8] Of interest are species with three or more accessible states that enable more complex logic processes in molecular electronics and spintronics[1,9-10] and potential high density ternary data storage which scales as 3^n rather than 2^n for binary data.[11-13]

Multiswitchable materials manifest transitions with two or more steps. Multistep transitions of molecular origin may be accessed with molecules on surfaces, in solution or as non-crystalline materials, and are therefore more versatile than traditional multistep switchable materials that depend on crystallographically-unique complexes or interactions in extended solids.[6,14-15] A simple example of a two-step interconversion in a molecular species is a dinuclear metal complex that exhibits spin crossover (SCO) at each of the metal centers.[16] The origin of the two-step transitions in dinuclear Fe(II) has been investigated extensively and has been linked to the use of constrained ligands to increase electronic communication,[17] intermolecular interactions[18-21] and the stability of the mixed low spin-high spin state.[22] The current understanding is that small changes in one metal site upon SCO at the other site are insufficient to give rise to the

two-step interconversion,[19,22] and instead the transition profile is directed by local electronic effects, which are difficult to control.[22]

Alternative switchable molecules include those that display valence tautomerism (VT): the reversible stimulated intramolecular electron transfer between a redox-active metal and a redox-active ligand.[23] The most common VT transition occurs with cobalt and 1,2-dioxolene ligands where cobalt may exist in the Co(II) or Co(III) oxidation state and the dioxolene is typically in the catecholate (cat^{2-}) or semiquinonate ($SQ^{\bullet-}$) redox forms. In these systems the octahedral low-spin (LS) Co(III) center undergoes a spin transition upon reduction to give high-spin (HS) Co(II) and so there exists an VT equilibrium between the {Co^{III}-cat} (Co^{III} = LS-Co(III)) and {Co^{II}-SQ} (Co^{II} = HS-Co(II)) states. The cobalt-dioxolene valence tautomeric transition is entropy-driven and has been induced by stimuli including temperature, light and pressure, resulting in changes in color, magnetic moment and polarization.[24-27] Valence tautomeric molecules have been attached to a metal surface and incorporated into thin films while retaining their switchable properties.[6,28-29]

Dinuclear VT complexes are candidates for two-step molecular transitions, and theoretical studies indicate these could be used as a two-qubit quantum gates in quantum information processing,[30] or as molecular switches in molecular electronics or spintronics due to their state-dependent conduction properties.[31] The profile of the magnetic transition (Figure 1) is expected to be affected by the electronic communication between the two Co-dioxolene units, which can be controlled for dinuclear bis(dioxolene)-bridged VT systems. This contrasts with the lack of control in Fe(II) SCO systems. One such example is $[\{Co(Me_2tpa)\}_2(diox\text{-}S\text{-}diox)]^{2+}$, (diox-S-diox = 6,6′-((1,4-phenylenebis(methylene))bis(sulfanediyl))bis(3,5-di-*tert*-butyl-benzene-1,2-diol; Chart S1), where the absence of electronic communication across the bis(dioxolene)-bridging ligand results in a concerted one-step two-electron VT transition (Figure 1).[32] A second influencing factor is the

matching of the cobalt and dioxolene redox potentials, which must also be considered for a VT transition to occur.[33-34] The cobalt redox potential is modulated by the ancillary ligand – for example, successive methylation in the 6-positions of the pyridyl rings of tris(pyridylmethyl)amine (Me_ntpa, n = 0–3) will increase the Co(III/II) reduction potential.[33,35] The dinuclear complex $[\{Co(bpy)_2)\}_2(thM)]^{2+}$ (bpy = 2,2′-bipyridine; $thMH_4$ = 3,3′,4,4′-tetrahydroxy-5,5′-dimethoxybenzaldazine; Chart S1) provides one example of the importance of the ancillary ligand: here the excessive stabilization of the Co(III) state by the bpy ligand affords the onset of a transition only evident at the highest measured temperatures.[36]

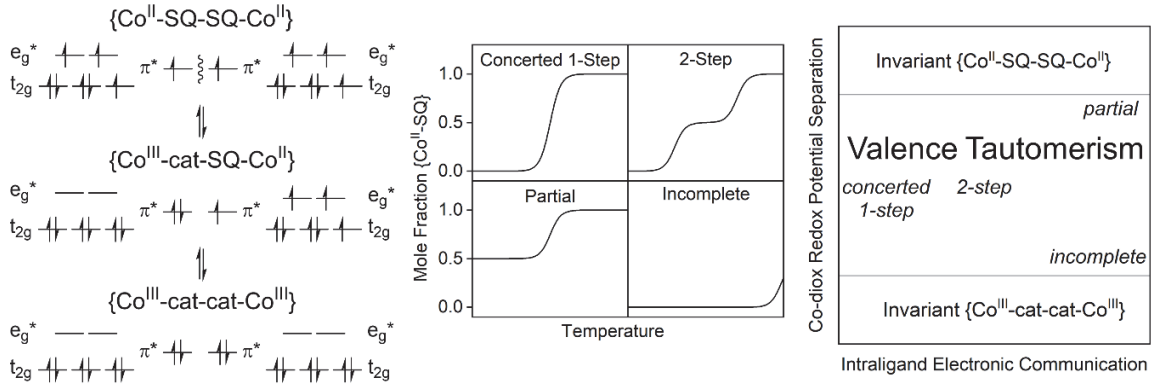

Figure 1. Schematic of valence tautomeric transitions in dinuclear cobalt-dioxolene complexes showing (left) the electronic states associated with a two-step transition, (center) the profiles of complete one-step, complete two-step, partial and incomplete transitions, and (right) the aim to relate the transition profile of a complex to its electronic communication and redox properties.

The target two-step VT transition in a dinuclear bis(dioxolene)-bridged complex occurs via a single-molecule mixed-valence $\{Co^{III}$-cat-SQ-$Co^{II}\}$ intermediate (Figure 1, left).[18] A two-step

transition could also be observed for a mixture of complexes in the {Co^{III}-cat-cat-Co^{III}} and {Co^{II}-SQ-SQ-Co^{II}} states (usually 1:1).[37] In addition, partial, one-electron-one-step VT transitions are possible (Figure 1), in which a transition is observed between the {Co^{II}-SQ-SQ-Co^{II}} state at high temperature and either the {Co^{III}-cat-SQ-Co^{II}} state or a 1:1 mixture of {Co^{III}-cat-cat-Co^{III}}:{Co^{II}-SQ-SQ-Co^{II}} at low temperature.

The only example of a two-step VT transition for a dinuclear cobalt complex with a bridging bis(dioxolene) ligand was reported by some of us in 2012.[38] The complex $[\{Co(Me_2tpa)\}_2(spiro)]^{2+}$ (**1**$^{2+}$; $spiroH_4$ = 3,3,3′,3′-tetramethyl-1,1′-spirobi(indan)-5,5′,6,6′-tetraol; Chart S1) shows two-step VT in both solution and solid states as measured by variable temperature UV-Vis spectroscopy and magnetic susceptibility, respectively.[35] The observation of VT in solution confirms that for **1**$^{2+}$ the VT interconversion is molecular in origin, corresponding to individual transitions at the Co-dioxolene moieties: {Co^{III}-cat-cat-Co^{III}} ⇌ {Co^{III}-cat-SQ-Co^{II}} ⇌ {Co^{II}-SQ-SQ-Co^{II}}. It was suggested that the two-step behavior of **1**$^{2+}$ could be the result of the temperature-dependent delocalization of an unpaired electron over the spiro ligand which is linked to an unidentified vibronic mode.[35]

In this work, we aimed to synthesize dinuclear cobalt bis(dioxolene) complexes to elucidate the parameters that influence the system to display one- or two-step VT transitions. For the synthesis of new dinuclear VT compounds, we selected the proligand 3,3,3′,3′-tetramethyl-1,1′-spirobi(indan)-4,4′,7,7′-tetrabromo-5,5′,6,6′-tetraol ($Br_4spiroH_4$). The Br_4spiro ligand presents shifted redox behavior with respect to the parent spiro ligand, affording useful insights into how redox properties effect the VT transition. The Me$_n$tpa ancillary ligands were chosen to provide a direct comparison with **1**$^{2+}$ and to allow access to an isostructural family in which the redox properties of cobalt can be matched to Br_4spiro. This gives rise to the target complexes

[{Co(Me$_n$tpa)}$_2$(Br$_4$spiro)]$^{2+}$ (Chart 1) where n = 0, 2, 3 (**2**$^{2+}$, **3**$^{2+}$ and **4**$^{2+}$, respectively), which are potential VT complexes. The hexafluorophosphate salts (**2a**, **3a** and **4a**) were synthesized in addition to the perchlorate salt, **2b**. The original two-step VT complex was isolated as the perchlorate salt (**1b**); for comparison to **2a**–**4a**, we report in this work the hexafluorophosphate salt, [{Co(Me$_2$tpa)}$_2$(spiro)](PF$_6$)$_2$ (**1a**). Zinc(II) analogs [{Zn^{II}(Me$_3$tpa)}$_2$(Br$_4$spiro$^{cat\text{-}SQ}$)](PF$_6$) (**5a**) and [{Zn^{II}(Me$_3$tpa)}$_2$(Br$_4$spiro$^{SQ\text{-}SQ}$)](PF$_6$)$_2$ (**6a**) were also been synthesized to facilitate the exploration of electronic communication properties of Br$_4$spiro without the complication of redox-activity in the metal centers.

Chart 1. Dinuclear metal complexes based on Br$_4$spiro and numbering scheme. R = H or Me for Me$_n$tpa; n = 0, 2 or 3.

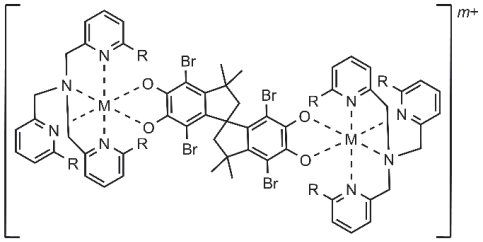

1a [{Co(Me$_2$tpa)}$_2$(spiro)](PF$_6$)$_2$
1b [{Co(Me$_2$tpa)}$_2$(spiro)](ClO$_4$)$_2$
2a [{Co(tpa)}$_2$(Br$_4$spiro)](PF$_6$)$_2$
2b [{Co(tpa)}$_2$(Br$_4$spiro)](ClO$_4$)$_2$
3a [{Co(Me$_2$tpa)}$_2$(Br$_4$spiro)](PF$_6$)$_2$
4a [{Co(Me$_3$tpa)}$_2$(Br$_4$spiro)](PF$_6$)$_2$
5a [{Zn(Me$_3$tpa)}$_2$(Br$_4$spiro)](PF$_6$)
6a [{Zn(Me$_3$tpa)}$_2$(Br$_4$spiro)](PF$_6$)$_2$

The detailed multi-technique experimental and DFT studies of the Co compounds and their Zn analogues presented herein have allowed attribution of the VT profile (two-step, concerted one-step, partial or incomplete) to a function of the bis(dioxolene) intraligand electronic communication and cobalt-dioxolene redox separation (Figure 1, right) and determination of the origin of two-step *versus* partial VT. We have quantified the ideal degree of electronic communication in the bis(dioxolene) bridging ligands by studying the mixed valence (MV) class of the $(cat\text{-}SQ)^{3-}$ ligand state. Finally, we propose simple guidelines as a basis for future efforts to achieve two-step VT compounds.

SYNTHESIS

The dinuclear cobalt compounds **1a**, **2a**, **3a** and **4a** were prepared under a nitrogen atmosphere by combining two equivalents of cobalt(II) chloride and the ancillary ligand in methanolic solution with one equivalent of bis(dioxolene) ligand and four equivalents of triethylamine dissolved in methanol. The resulting solution was concentrated under reduced pressure and then bubbled with compressed air for a minimum of 30 mins (Br_4spiro complexes) or until no further color change was observed. The cobalt complexes were precipitated by addition of a saturated aqueous potassium hexafluorophosphate solution. Bulk samples of grey-green **1a**·CH_2Cl_2 and tan-colored **3a** were obtained by layering of a dichloromethane solution with diethyl ether, while single crystals of **3a** were grown from dichloromethane/1,4-dioxane layering. Compounds **2a**·$4H_2O$ and **4a**·H_2O were obtained by recrystallization from hot methanol and ethanol to give light and dark green microcrystalline solids, respectively. Single crystals were grown from the same solvents.

The perchlorate salt of $\mathbf{2}^{2+}$ was also targeted due to the straightforward synthesis of $(H_3tpa)(ClO_4)_3$. The synthesis of compound **2b** was adapted from the synthesis of $[\{Co(tpa)\}_2(spiro)](ClO_4)_2\cdot 6H_2O$, using $Br_4spiroH_4$ in the place of $spiroH_4$ and 2.2 equivalents of triethylamine to deprotonate $Br_4spiroH_4$.[35] The green compound $\mathbf{2b}\cdot 3H_2O$ was recrystallized from acetone/hexane vapor diffusion, while diamond- ($\mathbf{2b_{pp}}\cdot$7acetone) and hexagonal- ($\mathbf{2b_{pd}}\cdot$3.9acetone) shaped green crystals of diffraction quality were obtained from acetone/hexane or acetone/cyclohexane vapor diffusion. Subscripts *pp* and *pd* label the geometric isomer present (detailed in SI). Low resolution PXRD indicate $\mathbf{2a}\cdot 4H_2O$ and $\mathbf{2a}\cdot$2.5MeOH have the same structure, while the bulk sample of $\mathbf{2b}\cdot 3H_2O$ is a mixture of $\mathbf{2b_{pp}}$ and $\mathbf{2b_{pd}}$ (Figures S1–S2).

Synthesis of zinc compound **5a** followed a similar procedure to compound **4a** above, with zinc(II) acetate used in the place of the cobalt salt and the reaction performed in aerobic conditions. Bubbling with compressed air was performed for a minimum of 1 h and the resultant suspension was filtered before precipitation of **5a** with aqueous potassium hexafluorophosphate. The crude product was recrystallized twice from acetone/diethyl ether layering to give $\mathbf{5a}\cdot 4.4H_2O$ a bright green microcrystalline solid, while single crystals were obtained by slowly evaporating an acetone/toluene solution. Compound **6a** was synthesized by sonicating compound **5a** with exactly one equivalent of ferrocenium hexafluorophosphate suspended in toluene.[39] Compound $\mathbf{6a}\cdot$0.5tol was obtained as brown-green powder from acetone/toluene layering, and single crystals of diffraction quality were obtained by layering a dichloromethane solution with toluene. Solvation of all compounds was confirmed by elemental analysis and thermogravimetric analysis (Figure S4).

INFRARED ABSORPTION SPECTROSCOPY

Infrared (IR) absorption spectra of **1a**–**6a** and **1b**–**2b** are reported in Figures S5–S7, with tabulated data and assignments in Table S4. The IR spectra confirm that complex $\mathbf{1}^{2+}$ in **1a** is isostructural with the complex in the previously reported perchlorate analog, **1b** (Figure S5);[35] likewise the cobalt complexes in **2a**·4H_2O and **2b**·3H_2O are isostructural (Figure S6). Previous combined DFT and transient IR studies enable the elucidation of ligand charge distributions from IR spectra.[40-41] The presence of catecholate bands (~1235, 1270 and 1329 cm^{-1}) in the IR spectra of **2a**·4H_2O, **2b**·3H_2O and **3a** (Figures S6–S7, Table S4) suggest a ligand charge distribution of $(cat\text{-}cat)^{4-}$ at room temperature. Compounds **4a**·H_2O and **6a**·0.5tol display bands characteristic of semiquinonate moieties (1455 cm^{-1}) at room temperature, consistent with a $(SQ\text{-}SQ)^{2-}$ ligand charge distribution. Bulk samples of compounds **1a**·CH_2Cl_2 and **5a**·4.4H_2O contain signature IR bands of both the catecholate and semiquinonate moieties (Figures S5 and S7, Table S4), indicative of an active VT interconversion in **1a**·CH_2Cl_2 at room temperature and a mixed-valence $(cat\text{-}SQ)^{3-}$ ligand charge distribution in **5a**·4.4H_2O. Compound **5a** therefore consists of a monocationic complex balanced by a single PF_6^- anion; this is confirmed by less intense PF_6^- bands (845 and 557 cm^{-1}) in the IR spectrum of **5a** compared to **2a**–**4a** and **6a** (Figure S7).

STRUCTURE DESCRIPTION

The solid-state structures of $Br_4spiroH_4$·2Et_2O, **2a**, **2b**, **3a**, **4a**, **5a** and **6a** were determined by single crystal X-ray diffraction, ($\mathbf{4}^{2+}$ is shown in Figure 2; crystallographic data, additional images and further discussion are provided in the Supporting Information). It was not possible to obtain single crystals of diffraction quality for any salt of $\mathbf{1}^{2+}$.[35] The cationic complexes $\mathbf{2}^{2+}$–$\mathbf{6}^{2+}$ consist of two

metal atoms bridged by the Br_4spiro bis(dioxolene) ligand, with each metal center capped by a the tripodal tetradentate Me_ntpa (n = 0, 2, 3) ligand. Due to the inequivalence of the O1 and O2 oxygen atoms of Br_4spiro (Figure 2), geometric isomerization is possible.[35] Compounds **2a**–**4a** crystallize with a C_2 axis running through the central spirocyclic carbon (C11) and a *proximal* geometry at the two crystallographically equivalent metal centers (*pp* isomer; see Supporting Information for naming convention). For compound **2b** we obtained crystal structures of two geometric isomers, *pp* and *pd* (*d* = *distal*), while **5a** and **6a** crystallize as *pp* and *pd* isomers respectively. Compounds **2b**, **5a** and **6a** do not possess any molecular symmetry. In compound **3a** the two methyl groups of Me_2tpa were approximately evenly disordered over three sites.

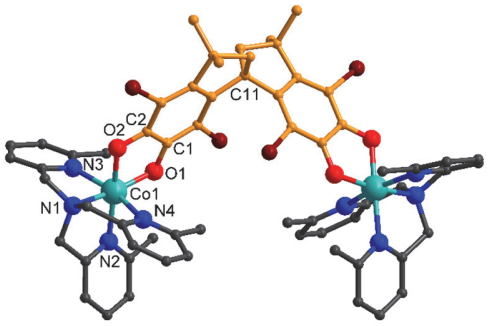

Figure 2. Complex cation in **4a**·2EtOH at 100 K. Color code: carbon on Me_3tpa, black; carbon on Br_4spiro, orange; oxygen, red; nitrogen, blue; cobalt, aqua green; bromine, brown. Hydrogen atoms have been omitted for clarity.

The presence of counterions and solvent in the crystal structures are consistent with the formulas **2a**·2.5MeOH, $\mathbf{2b_{pp}}$·7acetone, $\mathbf{2b_{pd}}$·3.9acetone, **3a**·4.5dioxane, **4a**·*x*EtOH (*x* = 2–3),

5a·2tol and **6a**·tol (Chart 1). The crystal structure formulae differ from the bulk recrystallized compounds which analyzed as **2a**·4H_2O, **2b**·3H_2O, **3a**, **4a**·H_2O, **5a**·4.4H_2O and **6a**·0.5tol; this is attributed to different solvent combinations required to obtain homogeneous bulk samples and the exchange of crystallization solvent with water on standing. Low resolution PXRD (Figure S3) shows **4a**·H_2O has the same packing as **4a**·*x*EtOH but with ethanol solvate in the channels having been exchanged for water.

To determine the cobalt oxidation state, we used the Co-O, Co-N_{amine} (N1 = N_{amine}) and Co-N_{py} (N2–N4 = N_{py}) bond lengths and octahedral distortion parameters (Σ, Θ and octahedral *SHAPE* index).[42-43] The *SHAPE* index calculated in SHAPE 2.1 represents the distortion of a coordination environment from an ideal polyhedron.[44-45] Cobalt(III) has short metal-ligand bonds and highly octahedral geometries compared to Co(II).[34,46] Typical parameters for Co^{III}/Co^{II} with Me*n*tpa ligands are 1.85–1.91/1.99–2.11 Å for Co-O, 1.91–1.97/2.09–2.13 Å for Co-N_{amine}, 1.87–2.03/2.14–2.29 Å for Co-N_{py} and 0.1–0.5/1.4–1.8 for the octahedral *SHAPE* index.[33-35] The dioxolene C-C and C-O bond lengths are correlated to the ligand oxidation state (Carugo *et al.*),[47] such that a least-squares fit enables assignment of an apparent metrical oxidation state (MOS, Brown *et al.*).[48] Catecholate ligands have a MOS of around –2 (*c.f.* SQ = –1), longer C-O bonds and shorter C1-C2 bonds. Based on the parameters given in Tables S6–S7, **2a**, **2b** and **3a** are assigned the charge distribution {Co^{III}-cat-cat-Co^{III}} in the solid state at low temperature (100 and 130 K). Compound **6a** has a {Zn^{II}-SQ-SQ-Zn^{II}} charge distribution, and compound **5a** is assigned a {Zn^{II}-cat-SQ-Zn^{II}} charge distribution at 100 K based on intermediate MOS values and bond lengths between those of **3a** and **6a** (Table S6). The dioxolene sites in **5a** are indistinguishable; the SQ/cat redox states are crystallographically disordered or electronically delocalized. The low

temperature crystallographic charge distributions of **2a**, **2b**, **3a**, **5a** and **6a** are consistent with the room temperature IR data.

At 300 K, the Co-O/N bond lengths and distortion parameters for **4a**·*x*EtOH unequivocally confirm a {Co^{II}-SQ-SQ-Co^{II}} charge distribution, consistent with the room temperature IR spectrum (Figure 3, Table S8).[35,46] On cooling, there is a contraction of Co-O/N bond lengths by 0.07–0.14 Å, which indicates VT transition. The unit cell parameters and cell volume slightly contract, which is reproduced in variable-temperature PXRD of the bulk sample (Figure S3 and S13). At 100 K, the bond lengths and octahedral distortion parameters at the cobalt site are intermediate between HS-Co(II) and LS-Co(III) values. The C-O bonds, C1-C2 bond and MOS value of –1.4(1) are also halfway between catecholate and semiquinonate values. Thus, single crystals of **4a**·*x*EtOH undergo a partial temperature-induced VT transition (Figure 1) between a {Co^{III}-cat-SQ-Co^{II}} charge distribution at 100 K, in which the two cobalt centers are crystallographically equivalent, and a {Co^{II}-SQ-SQ-Co^{II}} tautomer at 300 K. Crystallographic symmetry is maintained across the temperature range, suggesting a {Co^{III}-cat-SQ-Co^{II}} ⇌ {Co^{II}-SQ-SQ-Co^{II}} equilibrium rather than a {Co^{III}-cat-cat-Co^{III}} ⇌ {Co^{II}-SQ-SQ-Co^{II}} transition in 50% of molecules.[20] The partial VT transition in **4a**·*x*EtOH does not result in a dramatic change in the geometry of the complex (Figure S14).

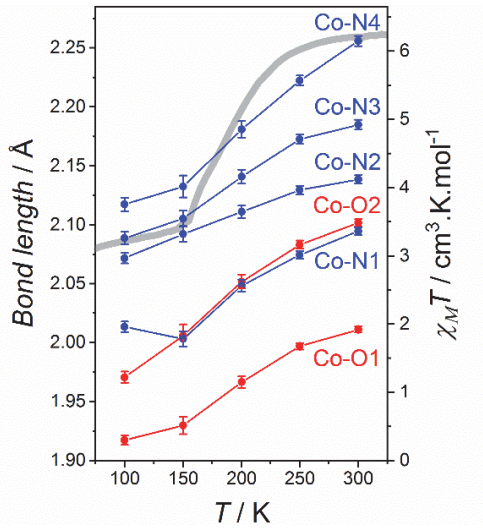

Figure 3. Temperature dependence of the Co-O (red) and Co-N (blue) bond lengths for **4a**·*x*EtOH (left axis) overlaid with the magnetic susceptibility data ($\chi_M T$) measured for **4a**·H_2O (grey, right axis) from Figure 4.

MAGNETIC MEASUREMENTS

Variable-temperature magnetic susceptibility data for compounds **1a**–**4a** are plotted as $\chi_M T$ vs T in Figure 4, where χ_M is the molar magnetic susceptibility. Compound **2a**·4H_2O shows temperature-independent paramagnetism typical for Co(III) ions[49] and a temperature-independent {Co^{III}-cat-cat-Co^{III}} charge distribution that agrees with crystallographic studies.

At low temperatures, compound **3a** is diamagnetic, with a $\chi_M T$ value of less than 0.06 cm^3 K mol^{-1} between 2 and 275 K. The low temperature charge distribution is therefore {Co^{III}-cat-cat-Co^{III}}, also consistent with the crystal structure of **3a**·4.5dioxane at 100 K. On the first heating cycle, the value of $\chi_M T$ for **3a** increases above 275 K, first gradually and then more rapidly above

310 K, to reach a maximum value of 1.19 cm^3 K mol^{-1} at 360 K. The increase in $\chi_M T$ between 275 and 360 K is consistent with the onset of a VT transition that is far from complete at 360 K, with ~40% of the molecules attaining the {Co^{III}-cat-SQ-Co^{II}} charge distribution. Repeated heating-cooling cycles on **3a** reveal a more gradual VT transition (Figure S16), which is commonly observed in VT compounds and may be associated with a structural change.[34,50]

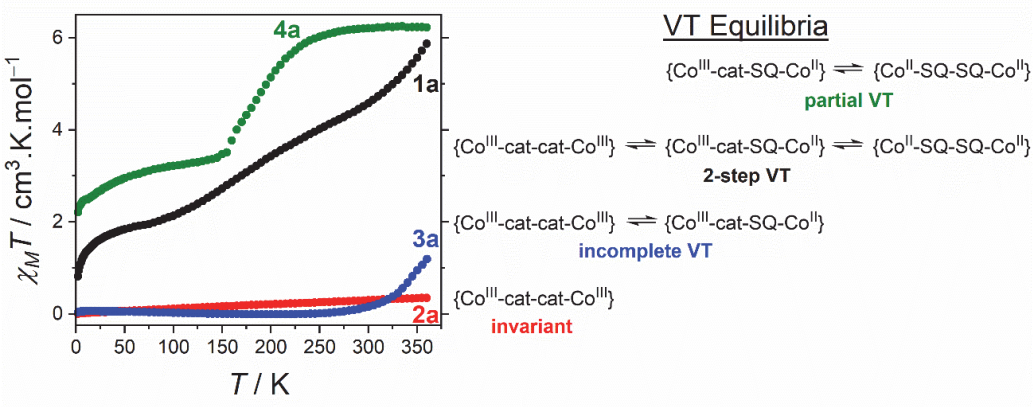

Figure 4. Plots of $\chi_M T$ vs T for the first heating of **1a**·CH_2Cl_2 (black); **2a**·$4H_2O$ (red), **3a** (blue) and **4a**·H_2O (green) and corresponding equations.

Compound **4a**·H_2O exhibits a $\chi_M T$ value of 6.23 cm^3 K mol^{-1} between 300 and 360 K, which is similar to other {Co^{II}-SQ-SQ-Co^{II}} complexes (6.15–7.37 cm^3 K mol^{-1})[32,35] and confirms the charge distribution observed in room temperature crystallography. The room temperature $\chi_M T$ value is within the range expected for two isolated or weakly-interacting spin-orbit coupled HS-Co(II)-SQ moieties (2.47–3.75 cm^3 K mol^{-1} each),[33,51] and is congruous with DFT calculations predicting weak coupling over the Br_4spiro bridging ligand (Table S17).

Compound **4a**·H_2O displays a single step transition between 140 and 300 K, which is more abrupt on the low-temperature side (Figure 4). The $\chi_M T$ value plateaus around 80–140 K at 3.1–3.4 cm^3 K mol^{-1}, which is approximately half of the high temperature value, before decreasing again to reach 2.21 cm^3 K mol^{-1} at 2 K. Repeated heating-cooling cycles are superimposable on the original heating curve (Figure S16). The magnetic data are consistent with a {Co^{III}-cat-SQ-Co^{II}} ⇌ {Co^{II}-SQ-SQ-Co^{II}} partial VT interconversion involving all molecules and centered at *Tc* = 190 K. The VT transition profile closely follows the variable temperature crystallography bond lengths (Figure 3) and the assignment of a partial transition is consistent with crystallography. The decrease in $\chi_M T$ at low temperature is due to the depopulation of the HS-Co(II)-SQ spin-orbit states and is commonly observed in HS-Co(II)-SQ complexes.[35,46,52-53]

Compound **1a**·CH_2Cl_2 displays a two-step VT transition, with a gradual first step in the range 70–300 K ($\chi_M T$ 1.93–4.57 cm^3 K mol^{-1}), and a more abrupt second step above 300 K reaching 5.87 cm^3 K mol^{-1} at 360 K (Figure 4). The $\chi_M T$ value at 70 K and the signature decrease on lowering temperature ($\chi_M T$ 0.82 cm^3 K mol^{-1} at 2 K) indicates that there is a trapped fraction of HS-Co(II)-SQ. The trapped fraction is estimated as ~25% {Co^{II}-SQ-SQ-Co^{II}} based on a maximum attainable $\chi_M T$ value of 7.37 cm^3 K mol^{-1} as measured for [{$Co^{II}(Me_3tpa)$}$_2$(spiro$^{SQ\text{-}SQ}$)]$(ClO_4)_2$.[35] The maximum attainable $\chi_M T$ values are significantly different in **1a** and **4a**, but this is compatible with both the cobalt single-ion contribution and the exchange interaction in the HS-Co(II)-SQ unit being highly sensitive to molecular geometry.[46] The magnetic data for **1a** are consistent with the remaining ~75% of molecules undergoing the first {Co^{III}-cat-cat-Co^{III}} ⇌ {Co^{III}-cat-SQ-Co^{II}} step VT interconversion between 70 and 300 K. The molecules then undergo an incomplete second {Co^{III}-cat-SQ-Co^{II}} ⇌ {Co^{II}-SQ-SQ-Co^{II}} step above 300 K such that ~60% of molecules reach the {Co^{II}-SQ-SQ-Co^{II}} state. Further cooling-heating cycles show a more gradual transition

(Figure S16) which is consistent with a structural change upon potential solvent loss.[35,54] The overall magnetic behavior of **1a** is similar to that of the previously reported perchlorate analog, **1b**, with both datasets showing a two-step VT transition but with compound **1a** displaying a larger trapped HS-Co(II)-SQ fraction than compound **1b**.[35] The thermal VT behavior is summarized in Figure 4.

ELECTRONIC ABSORPTION SPECTROSCOPY

Electronic absorption spectra were recorded for acetonitrile (MeCN) solutions of compounds **1a**–**6a** and are presented in Figure 5 with absorption bands and assignments tabulated in Table S11. Solution stability results are shown in Figures S17–S18: **1a** is stable in MeCN solution in a nitrogen atmosphere and **2a**–**6a** are stable in aerobic MeCN solution. The visible absorption spectrum of **1a** appears identical to the one reported for **1b** previously, indicating the counterion does not significantly affect the spin state in solution.[35] The charge distribution of **1a** is therefore predominately {Co^{II}-SQ-SQ-Co^{II}} at 298 K in MeCN.

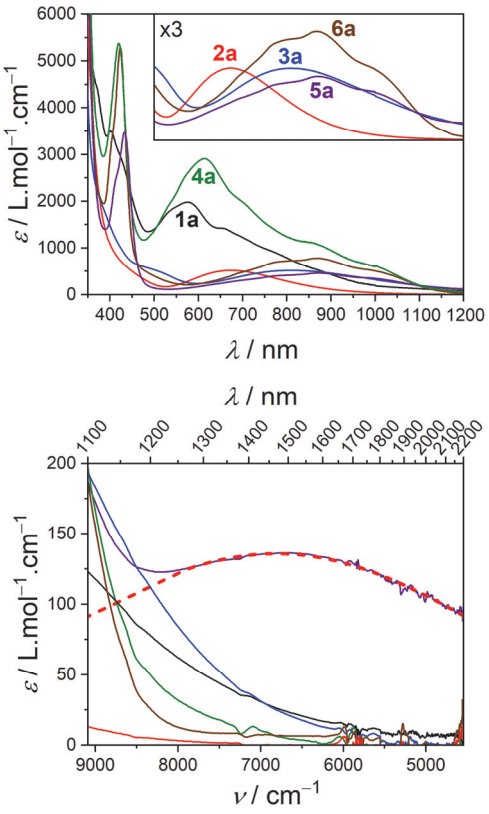

Figure 5. UV-Vis (top) and NIR (bottom) absorption spectra for acetonitrile solutions of **1a** (black), **2a** (red), **3a** (blue), **4a** (green), **5a** (purple) and **6a** (brown) at 298 K. Red dashed line indicates fitting of IVCT as described in the Supporting Information.

The visible absorption spectra of **2a** and **3a** are characteristic of LS-Co(III)-cat species and confirm the solid state {Co^{III}-cat-cat-Co^{III}} charge distribution is retained in solution.[34] The spectra of **2a** and **3a** both display a ligand-to-metal charge transfer (LMCT) band at 674 nm and 809 nm, respectively.[55] The LMCT band is shifted to lower energies in **3a** due to the smaller separation of {Co^{III}(Me_ntpa)-cat} and {Co^{II}(Me_ntpa)-SQ} states for n = 2 than n = 0; this is consistent with the observation of solid-state VT in **3a** but not **2a**.

The spectra of **4a**, **5a** and **6a** exhibit ligand-centered Br$_4$spiro semiquinonate transitions at 420 nm and 650–1000 nm, which are more intense for **4a** and **6a** than for **5a**. The semiquinonate bands confirm the presence of two semiquinonate radicals in **4a** and **6a** but one radical in **5a**. Thus, **5a** and **6a** have solution charge distributions of {Zn^{II}-cat-SQ-Zn^{II}} and {Zn^{II}-SQ-SQ-Zn^{II}}, respectively. The spectrum of **4a** also displays a strong metal-to-ligand charge transfer band at 614 nm; this spectrum is characteristic of HS-Co(II)-SQ,[34,46] and indicates **4a** exists in the {Co^{II}-SQ-SQ-Co^{II}} state in MeCN solution at room temperature. The room temperature charge distributions of compounds **2a**–**6a** are therefore maintained between solid and solution states. Variable-solvent measurements indicate the charge distributions are unchanged for **1a**, **2a** and **4a** in tetrahydrofuran (THF) and **5a** in 1,2-dichloroethane and chlorobenzene (Figures S19–S21).

Inspection of the near infrared (NIR) absorption spectra of **1a**–**6a** (Figure 5) reveals that only complex **5a** exhibits a broad NIR absorption at 1494 nm. The NIR absorption is assigned to an intervalence charge transfer (IVCT) between the catecholate and semiquinonate moieties of **5a**. Fitting and analysis of the IVCT band of **5a** in MeCN (dielectric constant, κ = 37.5) and 1,2-dichloroethane (κ = 10.36) revealed a very weak solvent-dependence (detailed in the Supporting Information). This indicates a class II-III MV system that shows solvent averaging but electronic localization,[56-57] consistent with the observation of both catecholate and semiquinonate IR bands (Table S4). The electronic coupling parameter, H_{AB}, was estimated as 1990 cm^{-1} in MeCN (Equation S5),[58] with $2H_{AB}/\nu_{max}$ = 0.71, which is on the border of class II-III and class II localization (Table S13), consistent with the low intensity broad IVCT band.[59] The IVCT analysis suggests the Br$_4$spiro ligand in **5a** exhibits stronger electronic coupling than the unsubstituted spiro ligand, which has previously been reported to have both class I and class II mixed-valence behavior.[60-62]

ELECTROCHEMISTRY

The redox and electronic communication properties of the spiro and Br4spiro complexes were investigated by electrochemistry. Cyclic and rotating disk electrode (RDE) voltammograms were recorded for MeCN solutions of **1a**–**6a** (Figure 6 and S24) and THF solutions of **1a**, **2a** and **4a** (Figure S25). Midpoint potentials (E_m), peak-to-peak separations (ΔE_p), half-wave potentials ($E_{1/2}$) and limiting currents (i_L) are reported in Table 1 (MeCN) and Table S14 (THF). We report peak potentials (E_p) in the case of irreversible processes, which are identified as having ΔE_p larger than ferrocene under the same conditions (68–81 mV in MeCN, 80–98 mV in THF).

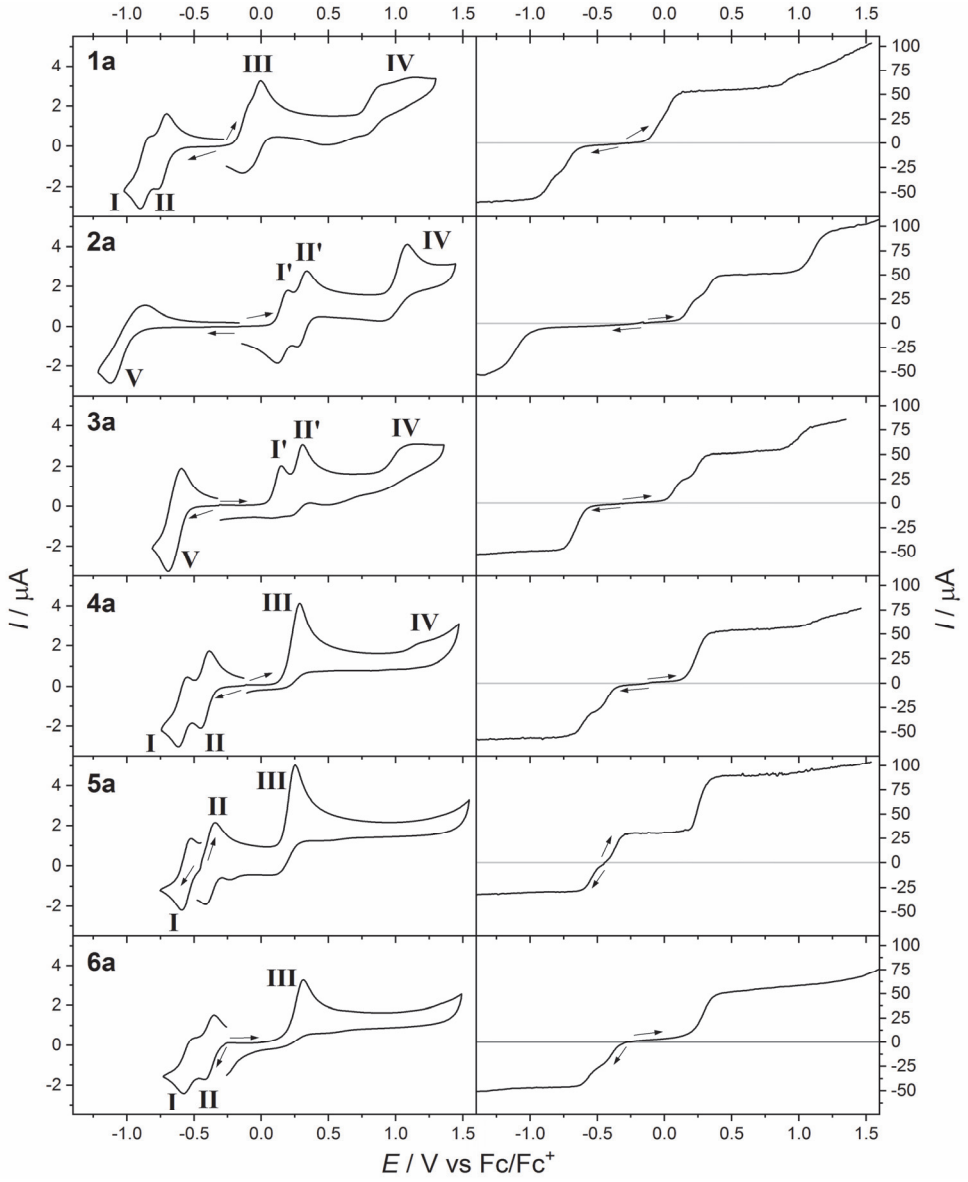

Figure 6. (Left) Cyclic voltammograms of acetonitrile solutions of compounds **1a**–**6a** (1.0 mM with 0.25 M Bu_4NPF_6) obtained with a scan rate of 100 mV s^{-1}. (Right) Corresponding RDE voltammograms at a scan rate of 50 mV s^{-1} and a rotation rate of 500 rotations min^{-1}. Arrows indicate the starting potential and direction of the scan.

Table 1. Cyclic voltammetry and rotating disk electrode voltammetry data for compounds **1a**–**6a** in acetonitrile[a]

	Cyclic Voltammetry Data					**Rotating Disk Electrode Voltammetry**				
	E_m **or** E_p **/ V (**ΔE_p **/ mV)**					$E_{1/2}$ **/ V (**i_L **/ µA)**				
	I/I′	**II/II′**	**III**	**IV**	**V**	**I/I′**	**II/II′**	**III**	**IV**	**V**
1a	–0.857 (88)	–0.739 (70)	–0.084 (155)	1.139 [b]	n/a	–0.875 (27.1)	–0.713 (27.2)	–0.011 (50.9)	-	n/a
2a	0.166 (69)	0.303 (74)	n/a	1.091 [b]	–0.993 (259)	0.178 (22.9)	0.328 (22.8)	n/a	1.100 (41.2)	–1.116 (48.1)
3a	0.149 [b]	0.307 [b]	n/a	1.159 [b]	–0.640 (92)	0.072 (23.7)	0.246 (23.6)	n/a	0.995 (22.5)	–0.660 (45.0)
4a	–0.583 (67)	–0.419 (65)	0.286 [b]	1.208 [b]	n/a	–0.614 (26.2)	–0.429 (26.3)	0.236 (49.3)	-	n/a
5a	–0.558 (70)	–0.383 (70)	0.250 [b]	n/a	n/a	–0.539 (28.5)	–0.368 (29.9)	0.255 (58.2)	n/a	n/a
6a	–0.533 (90)	–0.387 (74)	0.318 [b]	n/a	n/a	–0.560 (21.4)	–0.389 (22.5)	0.283 (44.4)	n/a	n/a

[a] 1.0 mM in acetonitrile with 0.25 M Bu_4NPF_6, scan rate 100 mV s^{-1}. Potentials reported versus Fc/Fc^+ couple. Error in potentials is ±5 mV. [b] E_p rather than E_m.

The cyclic voltammograms of **1a**, **4a**, **5a** and **6a** display three redox events in the central potential region (Figure 6, Figure S25): two closely-spaced one-electron processes (**I** and **II**) and a two-electron process (**III**). The RDE position of zero current identifies **I** and **II** as reductions and **III** as an oxidation for compounds **1a**, **4a** and **6a**, which compares well with the previously reported electrochemistry of **1b**.[35] For compound **5a**, the position of zero current has shifted relative to **6a** so that process **I** is a reduction and **II** and **III** are oxidations. Processes **I** and **II** are chemically-reversible and diffusion-controlled in all four complexes, except for process **I** for **1a** and **6a** that is quasi-reversible. Process **III** is irreversible for **4a**–**6a**, quasi-reversible for **1a** in MeCN (ΔE_p = 155 mV) and reversible for **1a** in THF (ΔE_p = 129 mV).

The cyclic voltammograms of **2a** and **3a** exhibit three distinct redox events in the central potential region: two one-electron oxidations (processes **I′** and **II′**) and a 2e-reduction (process **V**), as confirmed by RDE voltammetry. For compound **2a**, oxidations **I′** and **II′** are diffusion-controlled and chemically reversible, while process **V** is quasi-reversible. For compound **3a**, oxidations **I′** and **II′** are irreversible and process **V** is diffusion-controlled and chemically reversible, with a peak-to-peak separation of 92 mV. Cobalt compounds **1a**–**4a** also exhibit an irreversible or quasi-reversible 2e-oxidation (process **IV**) at highly positive potentials.

Process **I**/**I′** and **II**/**II′** are defined as spiro/Br$_4$spiro ligand-based processes and process **V** is defined as cobalt-based as shown in Scheme 1.[35] Compound **5a** is again confirmed to have (cat-SQ)$^{3-}$ mixed-valence by the position of zero current. Going from **1a** to **4a**, process **I** and **II** are shifted by approximately +300 mV as the electron-withdrawing substituents make Br$_4$spiro easier to reduce than spiro.[60] The irreversibility of processes **I′** and **II′** for compound **3a**, suggest that the {Co^{III}(Me$_2$tpa)-SQ} species is unstable compared to {Co^{III}(tpa)-SQ}.[34] Process **III** appears at the same potential (±35 mV) in cobalt and zinc compounds **4a**–**6a** in MeCN and so is assigned as a ligand-based oxidation of the bis(semiquinone) ligand to the bis(quinone) for a dicationic complex (Scheme 1). Quinones are weakly coordinating, so the irreversibility of process **III** for **4a**–**6a** is consistent with dissociation of the {Co^{II}-Q-Q-Co^{II}}$^{4+}$ species formed (Q = quinone). It appears that the bis(quinone) oxidation state is more stable for the unsubstituted spiro ligand than with the electron withdrawing substituents on Br$_4$spiro, as process **III** shows some reversibility for **1a**. The assignment of process **IV** is discussed in the Supporting Information and is shown in Scheme 1. The identity of processes **I**/**I′**, **II**/**II′**, **IV** and **V** are consistent with DFT calculations, as detailed in the Supporting Information (Figures S26–S29).

Scheme 1. Assigned redox processes for compounds **1a**–**6a** (M = Co, Zn).

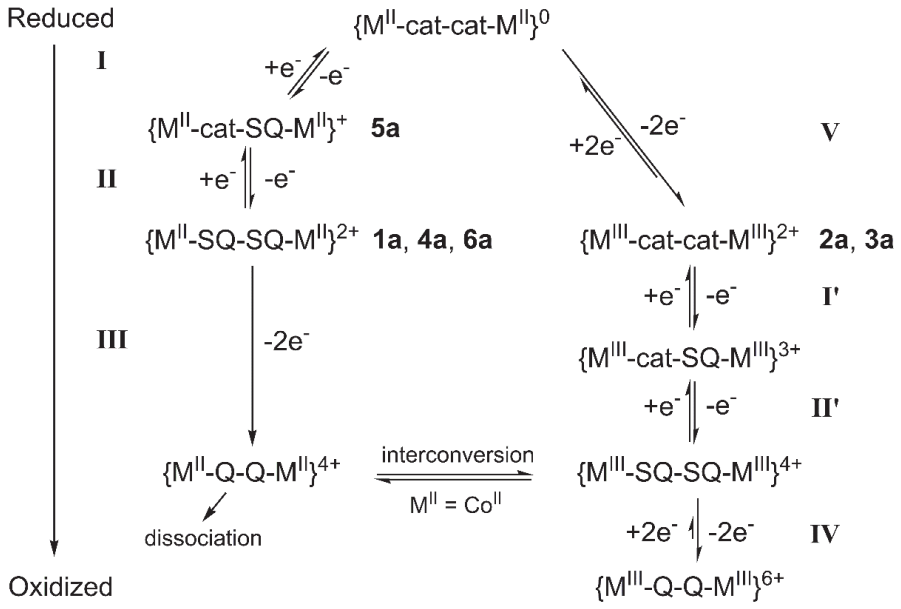

The mixed valence properties of bis(dioxolene) ligands and their H_{AB} values are roughly correlated with the separation between ligand redox processes **I** and **II**, termed Δ*diox* (Table 2).[63-64] Previously, Δ*diox* was measured for [{Co(Me$_n$tpa)}$_2$(spiro)](ClO$_4$)$_2$ (MeCN, 0.1 M Bu$_4$NPF$_6$), giving 143 mV for **1b** (*n* = 2) and 158–173 mV for *n* = 0, 1 and 3.[35] We find the class II-III MV compound **5a** to have the largest Δ*diox* value of 175 mV in MeCN (κ = 37.5, Table 2), followed by the partial VT compound **4a** and other Br$_4$spiro compounds, and finally the two-step VT compound **1a**. As the separation of redox potentials is solvent dependent;[65] we repeated the measurement for **1a**, **2a** and **4a** in non-polar THF (κ = 7.58) and found increased separations but the same ordering (**1a** < **2a** < **4a**; Table 2). We can conclude that the bridging ligand electronic communication in the bridging ligand increases **1a** < **2a** < **4a**. The MV class of **4a** is estimated as the upper end of class II or lower end of class II-III because of the similarity in Δ*diox* value to **5a**

and by comparison to Δ*diox* in bis(dioxolene) literature compounds (Table S13).[63-64] Without a spectroscopic handle, we cannot unequivocally assign the MV class for $(cat\text{-}SQ)^{3-}$ in **1a**–**4a**; however, the Δ*diox* value of **1a** is tentatively assigned as class II MV by comparison to literature values.[64] This is consistent with the rate of electron transfer in $[\{Co^{III}(tpa)\}_2(spiro^{cat\text{-}SQ})]^{3+}$ being on the EPR timescale ($\sim 10^{10}$ s^{-1}), slower than typical solvent reorientations ($\sim 10^{12}$–10^{13} s^{-1}).[35,57]

Table 2. Separation of electrochemical processes for compounds **1a–6a** [a]

	Acetonitrile		Tetrahydrofuran	
	Δ*diox*	**Δ*ox-red***	**Δ*diox***	**Δ*ox-red***
1a	120	~655 [b]	140	~810 [b]
2a	135	1160	180	1230
3a	160 [c]	790 [c]		
4a	165	~705 [b,c]	240	~850 [b,c]
5a	175	-		
6a	145	-		

[a] Calculated from CV potentials. Values reported in mV to the nearest 5 mV, error in parameters is ±10 mV. [b] An estimation of *Δox-red* as discussed in the text. [c] E_p used in calculation instead of E_m as oxidative processes are irreversible.

The parameter Δ*ox-red* is defined as the separation between the midpoint potentials of the (reversible) first 1e-oxidation and first 1e-reduction, in the case when one process is metal-based and the other ligand-based. In our previous work, we established the approximate rule Δ*ox-red* < 740 mV for VT to occur in a thermally accessible range for mononuclear VT compounds.[34] The value of Δ*ox-red* is well defined for $\{Co^{III}\text{-cat}\}$ species that undergo a cobalt reduction process (**V**).[39] Values of Δ*ox-red* in MeCN for **2a** and **3a** (Table 2) are consistent with the absence of VT in **2a** (Δ*ox-red* >> 740 mV) and the presence of an incomplete VT transition at high temperature

in **3a** (Δ*ox-red* ~ 740 mV). In compounds **1a** and **4a**, both first oxidation and reduction potentials are ligand-based and so Δ*ox-red* is not defined. In this case, we give the separation of ligand-based redox potentials for **II** and **III** as a rough estimate of Δ*ox-red*, given that {Co^{II}-Q-Q-Co^{II}} species may rearrange to form {Co^{III}-SQ-SQ-Co^{III}} (Table S15). The estimated Δ*ox-red* values in MeCN are consistent with both **1a** and **4a** displaying VT in the solid state (Table 2). Use of less polar THF results in increased potential separations but maintained trends: estimates of Δ*ox-red* for VT complexes **1a** and **4a** are still significantly less than for the non-VT complex **2a**. However, it is clear that the Δ*ox-red* criterion is solvent-dependent, and care must be taken to only compare measurements performed in the same solvent.

COMPUTATIONAL STUDY

Density functional theory calculations were performed for compounds **1a**, **2b**, **3a** and **4a** in the gas phase to examine their magnetic behavior (optimized structures and energies are given in the Supporting Information); **2b** was selected over **2a** to examine the effect of *pp* and *pd* geometric isomers. Valence tautomeric mononuclear complexes have been investigated with DFT in the past,[34,39,66-68] but to date DFT on dinuclear cobalt VT systems has only been used to predict VT transitions in hypothetical complexes.[69-71] To analyze dinuclear VT transitions we draw a parallel with DFT investigations of two-step SCO systems.[22,72] As such, all three charge distributions in a dinuclear complex can be considered to be in equilibrium. The nature of the transition is then described by the thermochemical parameter ρ, given by Equation (3) where state energies, E, are given relative to E{Co^{III}-cat-cat-Co^{III}}.

$$\rho = \frac{E\{\mathrm{Co^{III}\text{-}cat\text{-}SQ\text{-}Co^{II}}\} - {}^{1}/_{2}E\{\mathrm{Co^{II}\text{-}SQ\text{-}SQ\text{-}Co^{II}}\}}{E\{\mathrm{Co^{II}\text{-}SQ\text{-}SQ\text{-}Co^{II}}\}} \quad (3)$$

For the case that all three charge distributions are thermally accessible and $E\{\mathrm{Co^{III}}\text{-cat-cat-Co}^{\mathrm{III}}\} < E\{\mathrm{Co^{III}}\text{-cat-SQ-Co}^{\mathrm{II}}\} < E\{\mathrm{Co^{II}}\text{-SQ-SQ-Co}^{\mathrm{II}}\}$, $\rho > 0$ implies a two-electron-one-step VT transition: $\{\mathrm{Co^{III}}\text{-cat-cat-Co}^{\mathrm{III}}\} \rightleftharpoons \{\mathrm{Co^{II}}\text{-SQ-SQ-Co}^{\mathrm{II}}\}$. A two-step transition is favored for $\rho < 0$, with a more negative ρ value corresponding to a larger separation between the two steps. If $\{\mathrm{Co^{III}}\text{-cat-SQ-Co}^{\mathrm{II}}\}$ is the ground state ($\rho < -0.5$), the only possible VT transition is a partial transition $\{\mathrm{Co^{III}}\text{-cat-SQ-Co}^{\mathrm{II}}\} \rightleftharpoons \{\mathrm{Co^{II}}\text{-SQ-SQ-Co}^{\mathrm{II}}\}$ (Figure 1).

Density functional theory calculations on compound **1a** used the DFT-optimized geometry of **3a** as a starting point in the absence of a crystal structure. Calculations confirmed the $\{\mathrm{Co^{III}}\text{-cat-cat-Co}^{\mathrm{III}}\}$ charge distribution as the ground state, with both the $\{\mathrm{Co^{III}}\text{-cat-SQ-Co}^{\mathrm{II}}\}$ and $\{\mathrm{Co^{II}}\text{-SQ-SQ-Co}^{\mathrm{II}}\}$ charge distributions being thermally accessible, at 1.1 and 4.0 kcal mol^{-1}, respectively (Figure 7). This is consistent with the assignment of the experimentally observed two-step behavior as a two-step $\{\mathrm{Co^{III}}\text{-cat-cat-Co}^{\mathrm{III}}\} \rightleftharpoons \{\mathrm{Co^{III}}\text{-cat-SQ-Co}^{\mathrm{II}}\} \rightleftharpoons \{\mathrm{Co^{II}}\text{-SQ-SQ-Co}^{\mathrm{II}}\}$ VT transition of molecular origin. The parameter $\rho = -0.24$ is concordant with two well-separated interconversion steps.

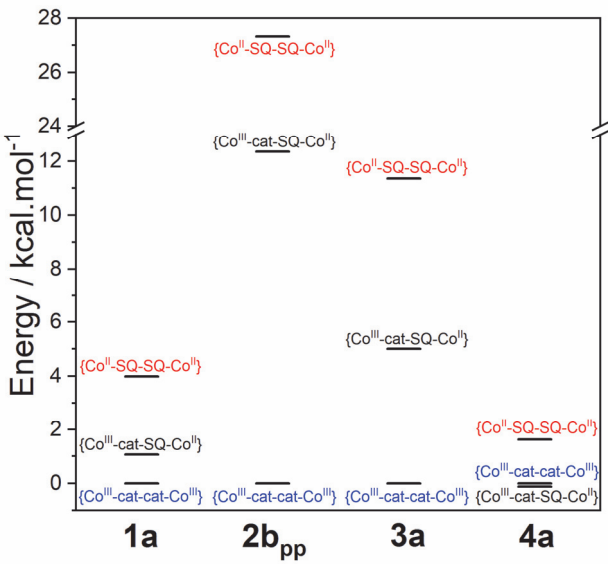

Figure 7. Schematic showing the relative energies of different electronic states of **1a**, **2b$_{pp}$**, **3a** and **4a** calculated by the DFT UTPSSh/6-311++G(d,p) method.

Calculations for compound **2b** revealed the **2b$_{pp}$** and **2b$_{pd}$** isomers to be approximately equal in energy (0.2 kcal mol^{-1}, Table S15) in the {Co^{III}-cat-cat-Co^{III}} charge distribution, and so further calculations focused on **2b$_{pp}$**. For **2b$_{pp}$**, the {Co^{III}-cat-cat-Co^{III}} charge distribution is predicted to be the ground state (Figure 7), in agreement with the experimental results. The Co-O/N and dioxolene bond lengths in **2b$_{pp}$** {Co^{III}-cat-cat-Co^{III}} closely reproduce the X-ray structure, **2b$_{pp}$**·7acetone (Figure S31). The {Co^{III}-cat-SQ-Co^{II}} and {Co^{II}-SQ-SQ-Co^{II}} charge distributions for **2b$_{pp}$** have relative energies of 12.3 kcal mol^{-1} and 27.3 kcal mol^{-1} respectively, and so are predicted to be thermally inaccessible (Figure 7). The DFT prediction is consistent with the temperature invariant {Co^{III}-cat-cat-Co^{III}} state for **2^{2+}**.

For compound **3a**, the ground state is the {Co^{III}-cat-cat-Co^{III}} charge distribution, with the next highest state being {Co^{III}-cat-SQ-Co^{II}} at 5.0 kcal mol^{-1}. The DFT calculations predict a

diamagnetic {Co^{III}-cat-cat-Co^{III}} ground state with a thermally-induced VT transition to the {Co^{III}-cat-SQ-Co^{II}} state, consistent with experiment. The {Co^{II}-SQ-SQ-Co^{II}} state is predicted to have a relative energy of 11.4 kcal mol^{-1} and is therefore unlikely to form in an accessible temperature range. However, the ρ-value for **3a** (and $\mathbf{2b_{pp}}$) is –0.06 (Table S16), which indicates that a two-step transition is expected at a sufficiently high temperature—the electronic properties of Br_4spiro are such that a two-step transition is possible for **3a** but is outside the experimentally-accessible temperature range.

Calculations on compound **4a** revealed the {Co^{III}-cat-cat-Co^{III}} and {Co^{III}-cat-SQ-Co^{II}} charge distributions to be isoenergetic (Table S16). However, the zero-point harmonic vibrations (Table S15) and spin degeneracy result in an entropic term that more favourably stabilizes the {Co^{III}-cat-SQ-Co^{II}} state. As thermally-induced VT is an entropy-driven process, no VT transition is expected between the {Co^{III}-cat-SQ-Co^{II}} and {Co^{III}-cat-cat-Co^{III}} charge distributions. The {Co^{II}-SQ-SQ-Co^{II}} charge distribution is higher in energy than the {Co^{III}-cat-SQ-Co^{II}} state by 1.7 kcal mol^{-1} (Figure 7). Thus, DFT calculations on **4a** predict a partial {Co^{III}-cat-SQ-Co^{II}} ⇌ {Co^{II}-SQ-SQ-Co^{II}} VT transition with ρ = –0.57.

The isotropic exchange coupling constants in the {Co^{III}-cat-SQ-Co^{II}} and {Co^{II}-SQ-SQ-Co^{II}} change distributions of **1a**, $\mathbf{2b_{pp}}$, **3a** and **4a** were calculated by the Broken Symmetry approximation.[73] The exchange interaction between unpaired electrons on the HS-Co(II) ion and the nearest (coordinating) semiquinone was calculated to be strongly ferromagnetic (Table S17), consistent with DFT calculations on the mononuclear complexes with Me_ntpa.[74] However, this interaction is known to be anisotropic with contributions from spin–orbit coupling that are not represented accurately by DFT calculations.[46] The calculated exchange interactions between the

other paramagnetic centers in the complex were negligible and within the error of the DFT method (Table S17).

DISCUSSION

Here we will attempt to correlate the observed solid-state VT behavior of dinuclear cobalt bis(dioxolene) complexes with the solution-state electrochemistry. This comparison neglects the effects of packing in the solid-state, which are important for dinuclear SCO complexes,[19-21] as well as the effects of solvent and electrolyte on electrochemistry, so we compare values recorded in MeCN with Bu_4NPF_6 where possible.[65] The evaluation is supported by the excellent agreement of gas phase DFT predictions and solid-state magnetic data as well as similar two-step VT interconversions being observed for solid **1a** and **1b** and for **1b** in solution.[35]

In the electrochemistry section, we discussed the correlation between Δ*ox-red* and the possibility of VT. The Δ*ox-red* parameter describes the energy match between the cobalt and dioxolene frontier orbitals; for a given bis(dioxolene) ligand, the ancillary ligand governs Δ*ox-red* by modulating the metal redox potential.[34] For compound **2a**, there is a mismatch of the $\{Co^{II}(tpa)\}/\{Co^{III}(tpa)\}$ and the $(cat\text{-}cat)^{4-}/(cat\text{-}SQ)^{3-}$ redox potentials, which results in a large Δ*ox-red* and a significant thermodynamic stabilization of the $\{Co^{III}\text{-}cat\text{-}cat\text{-}Co^{III}\}$ state. Thus, $\mathbf{2}^{2+}$ lies in the lower region of Figure 8 and displays a temperature-invariant $\{Co^{III}\text{-}cat\text{-}cat\text{-}Co^{III}\}$ state. In contrast, for $\mathbf{3}^{2+}$, there is a better, but still not ideal, match between the redox potentials in $\{Co^{II}(Me_2tpa)\}/\{Co^{III}(Me_2tpa)\}$ and $(cat\text{-}cat)^{4-}/(cat\text{-}SQ)^{3-}$, which means VT is possible (Figure 8) and occurs at high temperature. The choice of bis(dioxolene) can also affect Δ*ox-red*; in Figure 8

all Br4spiro complexes have more negative Δ*ox-red* values than the corresponding spiro compounds with the same ancillary ligand (**2**$^{2+}$ and **A**; **3**$^{2+}$ and **1**$^{2+}$; **4**$^{2+}$ and **C**).

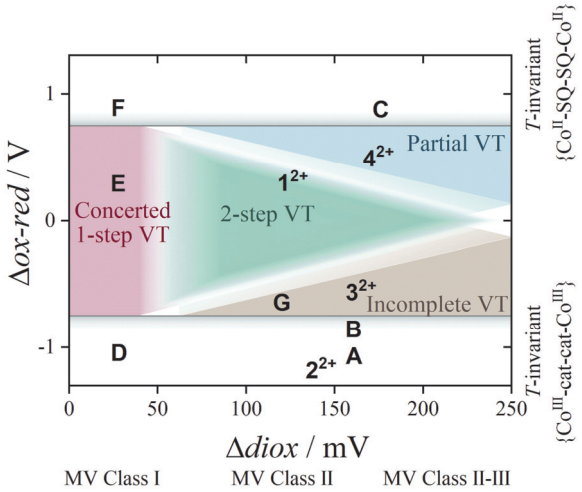

Figure 8. Correlation between redox parameters and VT transition characterstics for dinuclear cobalt bis(dioxolene) complexes. Electrochemical data are measured in MeCN (1 mM analyte concentrations with 0.10–0.25 M Bu_4NPF_6) and include **1**$^{2+}$–**4**$^{2+}$, $[\{Co(Me_ntpa)\}_2(spiro)]^{2+}$ (n = 0, 1, 3 is **A**, **B**, **C**),[35] $[\{Co(Me_ntpa)\}_2(diox\text{-}S\text{-}diox)]^{2+}$ (n = 0, 2, 3 is **D**, **E**, **F**; redox parameters estimated based on VT behavior)[32] and $[\{Co(bpy)_2\}_2(thM)]^{2+}$ (unspecified concentration in MeCN with ~0.1 M Bu_4NBF_4).[36]

The computational study indicates **4a** undergoes a partial transition because the {Co^{III}-cat-SQ-Co^{II}} state is stabilized relative to the {Co^{III}-cat-cat-Co^{III}} state. The redox potentials of the {Co^{II}(Me$_3$tpa)}/{Co^{III}(Me$_3$tpa)} (not directly observed) and (cat-SQ)$^{3-}$/(SQ-SQ)$^{2-}$ couples in **4a** are sufficiently close to enable the observed VT event: {Co^{III}-cat-SQ-Co^{II}} ⇌ {Co^{II}-SQ-SQ-Co^{II}}. Due to the strong Br4spiro-meidated electronic coupling in **4a** (tentatively MV class II-III), the

$(cat\text{-}SQ)^{3-}/(SQ\text{-}SQ)^{2-}$ and $(cat\text{-}cat)^{4-}/(cat\text{-}SQ)^{3-}$ redox couples are well separated, resulting in a large separation of the $(cat\text{-}cat)^{4-}/(cat\text{-}SQ)^{3-}$ and $\{Co^{II}(Me_3tpa)\}/\{Co^{III}(Me_3tpa)\}$ couples. This is interpreted as a large separation of $\{Co^{II}(Me_3tpa)\}/\{Co^{III}(Me_3tpa)\}$ and $(cat\text{-}cat)^{4-}$ orbital energies, consistent with destabilization of the $\{Co^{III}\text{-}cat\text{-}cat\text{-}Co^{III}\}$ state relative to the $\{Co^{III}\text{-}cat\text{-}SQ\text{-}Co^{II}\}$ ground state, causing complex $\mathbf{4}^{2+}$ to lie in the partial VT region of Figure 8.

We propose that for two-step VT to occur, the *d*-orbital energies of cobalt in $\{Co^{II}(L)\}$ and $\{Co^{III}(L)\}$ (L = ancillary ligand) must be similar to the ligand frontier orbital energies in all three of the $(cat\text{-}cat)^{4-}$, $(cat\text{-}SQ)^{3-}$ and $(SQ\text{-}SQ)^{2-}$ states. Similar orbital energies allow the three distinct charge distributions to be close in energy, and a two-step VT interconversion to be observed. For complex $\mathbf{1}^{2+}$, this can be considered as matching the potential of the $\{Co^{II}(Me_2tpa)\}/\{Co^{III}(Me_2tpa)\}$ redox couple (not directly observed) with both the $(cat\text{-}cat)^{4-}/(cat\text{-}SQ)^{3-}$ and $(cat\text{-}SQ)^{3-}/(SQ\text{-}SQ)^{2-}$ redox couples. The likelihood of the $\{Co^{II}(L)\}/\{Co^{III}(L)\}$ orbital energies (L = ancillary ligand) being sufficiently close to the orbital energies of all three dioxolene forms is enhanced when the dioxolene relative energies are close together (small $\Delta diox$), which gives rise to the triangular shape of the two-step VT region in Figure 8. This follows from our observations for **1a** and **4a**: the smaller electronic coupling and smaller $\Delta diox$ value for **1a** place it in the two-step region while the larger electronic coupling and $\Delta diox$ value place **4a** in the partial VT region. The smaller the electronic coupling, while remaining non-zero, the higher the likelihood of the complex lying in the two-step region.

The $\Delta diox$ parameter correlates with the stability of the mixed-valence state and the electronic coupling of the mixed-valence bis(dioxolene) ligand. We propose that when paired with the appropriate ancillary ligand (correct $\Delta ox\text{-}red$), class II bis(dioxolene) ligands (and class II-III bis(dioxolene) ligands with sufficiently weak coupling) are ideal as bridging ligands for two-step

VT. These ligands allow electronic communication between the two moieties but retain closely spaced redox potentials for the three ligand oxidation states. The first VT electron transfer shifts the redox potential for the second electron transfer so that the second VT step requires more energy than the first. This is equivalent to stabilizing the {Co^{III}-cat-SQ-Co^{II}} state relative to the average energy of the {Co^{III}-cat-cat-Co^{III}} and {Co^{II}-SQ-SQ-Co^{II}} states. In contrast, class I MV ligands with no intraligand electronic communication favor two-electron concerted one-step transitions and strongly coupled class II-III and class III ligands favor one-electron-one-step transitions. Bis(dioxolene) bridging ligands provide direct control over the electronic communication between the two VT centers and therefore control over the propensity for two-step VT.

CONCLUDING REMARKS AND FUTURE DIRECTIONS

Building upon past work that identified the first two-step VT transition in a dinuclear bis(dioxolene)-bridged cobalt complex, **1b**,[35,38] four new dinuclear cobalt compounds have been synthesized and investigated. One is the hexafluorophosphate analog of the original complex (**1a**) that also displays a two-step VT transition in the solid state. The other compounds are based on the Br_4spiro bridging ligand and Me_ntpa (n = 0, 2, 3) ancillary ligand (**2a**, **2b**, **3a** and **4a**). Complexes $\mathbf{2}^{2+}$ and $\mathbf{3}^{2+}$ display {Co^{III}-cat-cat-Co^{III}} charge distributions at room temperature in both solid and solution state, and compound **3a** exhibits the onset of a VT transition above 275 K in the solid state that is incomplete at the highest temperatures measured. Compound **4a** exhibits a partial VT transition {Co^{III}-cat-SQ-Co^{II}} ⇌ {Co^{II}-SQ-SQ-Co^{II}} centered at 190 K. In all cases, the structural, spectroscopic and magnetic data are fully consistent with DFT calculations, allowing unambiguous assignment of the charge distribution in the complex and electronic state

of the metal center. The DFT computational studies have also facilitated rationalization of the presence or absence of a VT transition and its stepwise characteristics.

The VT behavior of bis(dioxolene) cobalt complexes has been correlated with their redox properties to provide guiding principles for the development of two-step VT complexes (Figure 8). The guidelines laid out provide a predictive tool from which one can carefully choose the bis(dioxolene) and ancillary ligand to achieve two-step VT. Future efforts should target class II and class II-III MV bis(dioxolene) ligands with weaker intramolecular electronic coupling between the two dioxolene units than is the case for Br_4spiro. This intramolecular electronic coupling can be conveniently measured by the potential separation between dioxolene-based redox processes ($\Delta diox$) or via NIR spectroscopy. Matching these bridging ligands with appropriate ancillary ligands to tune $\Delta ox\text{-}red$ should enable access to new VT transitions with two closely-spaced steps, as observed for **1a**. Future attempts to synthesize two-step VT compounds could alternatively pair Br_4spiro with an ancillary ligand that gives cobalt a reduction potential between those imposed by Me_2tpa and Me_3tpa, such that the new complex may lie between $\mathbf{3}^{2+}$ and $\mathbf{4}^{2+}$ on Figure 8.

Here we have shown that the VT behavior and intramolecular electronic communication can be controlled in dinuclear cobalt complexes bridged by a redox-active ligand. Active control of dinuclear VT complexes represents a significant advantage over dinuclear SCO complexes where the occurrence of a two-step transition is influenced by local electronic effects that are difficult enough to predict computationally, let alone design.[22] The retention of two-step VT in **1a** and **1b** is a preliminary indication that two-step VT compounds are less affected by the surrounding chemical environment than dinuclear SCO compounds and may be better able to retain their two-step VT interconversion when employed in devices. Future work should focus on improving the abruptness of VT transitions to enable applications in macroscopic devices. Although there are

fewer examples of dinuclear VT compounds, they present a significant area of interest where the nature of the interconversion may soon be designed using simple chemistry principles.

ASSOCIATED CONTENT

Supporting Information. The supporting information is available free of charge online: Details of experimental and synthetic methods, IR, TGA, crystallographic, structural, PXRD, magnetic, Vis-NIR, electrochemical and DFT (PDF). X-ray crystallographic files for Br_4spiro$H_4\cdot 2Et_2O$, **2a**·2.5MeOH, $\mathbf{2b_{pp}}$·7acetone, $\mathbf{2b_{pd}}$·3.9acetone, **3a**·4.5dioxane, **4a**·*x*EtOH (*x* = 2–3; 100, 150, 200, 250 and 300 K), **5a**·2tol and **6a**·tol (CIF).

AUTHOR INFORMATION

Corresponding Author

*Email: c.boskovic@unimelb.edu.au

Present Address

[I] Department of Chemistry, School of Natural Sciences, The University of Manchester, Oxford Road, Manchester, M13 9PL, U.K.

Author Contributions

The manuscript was written through contributions of all authors. All authors have given approval to the final version of the manuscript.

Notes

The authors declare no competing financial interest.

ACKNOWLEDGMENT

We thank the Australian Research Council for financial support (DP150100353 and DP190100854) to CB. GKG acknowledges the support of an Elizabeth and Vernon Puzey Scholarship from the University of Melbourne, an Australian Government Research Training Award and a Postgraduate Student Travel Bursary from the Royal Australian Chemical Institute. We thank Tina Tezgerevska for synthesis of the ligand $(H_3tpa)(ClO_4)_3$, Dr Elodie Rousset for assistance with the synthesis of tpa and Ken Gransbury for help conceptualizing figures. This research was undertaken in part using the MX1 and MX2 beamlines at the Australian Synchrotron, part of ANSTO, and made use of the ACRF detector. AS thanks the Russian Science Foundation for financial support (19-73-00090). MPS and BNL thank the US National Science Foundation for financial support (NSF-CHE-1800554).

REFERENCES

1. Coronado, E., Molecular magnetism: from chemical design to spin control in molecules, materials and devices. *Nat. Rev. Mater.* **2020,** *5*, 87-104.
2. Dei, A.; Gatteschi, D., Molecular (Nano) Magnets as Test Grounds of Quantum Mechanics. *Angew. Chem., Int. Ed.* **2011,** *50*, 11852-11858.
3. Senthil Kumar, K.; Ruben, M., Emerging trends in spin crossover (SCO) based functional materials and devices. *Coord. Chem. Rev.* **2017,** *346*, 176-205.
4. Kahn, O.; Martinez, C. J., Spin-Transition Polymers: From Molecular Materials Toward Memory Devices. *Science* **1998,** *279*, 44-48.
5. Létard, J.-F.; Guionneau, P.; Goux-Capes, L., Towards Spin Crossover Applications. In *Spin Crossover in Transition Metal Compounds*, Springer: Berlin, Heidelberg, 2004; Vol. 235, pp 221-249.
6. Paquette, M. M.; Plaul, D.; Kurimoto, A.; Patrick, B. O.; Frank, N. L., Opto-Spintronics: Photoisomerization-Induced Spin State Switching at 300 K in Photochrome Cobalt–Dioxolene Thin Films. *J. Am. Chem. Soc.* **2018,** *140*, 14990-15000.

7. Bayliss, S. L.; Laorenza, D. W.; Mintun, P. J.; Diler, B.; Freedman, D. E.; Awschalom, D. D., Optically Addressable Molecular Spins for Quantum Information Processing. **2020**, arXiv:2004.07998. arXiv.org e-Print archive. https://arxiv.org/abs/2004.07998 (accessed May 10, 2020).
8. Dugay, J.; Giménez-Marqués, M.; Kozlova, T.; Zandbergen, H. W.; Coronado, E.; van der Zant, H. S. J., Spin Switching in Electronic Devices Based on 2D Assemblies of Spin-Crossover Nanoparticles. *Adv. Mater.* **2015,** *27*, 1288-1293.
9. Simão, C.; Mas-Torrent, M.; Casado-Montenegro, J.; Otón, F.; Veciana, J.; Rovira, C., A Three-State Surface-Confined Molecular Switch with Multiple Channel Outputs. *J. Am. Chem. Soc.* **2011,** *133*, 13256-13259.
10. Andréasson, J.; Pischel, U.; Straight, S. D.; Moore, T. A.; Moore, A. L.; Gust, D., All-Photonic Multifunctional Molecular Logic Device. *J. Am. Chem. Soc.* **2011,** *133*, 11641-11648.
11. Fortier, S.; Le Roy, J. J.; Chen, C.-H.; Vieru, V.; Murugesu, M.; Chibotaru, L. F.; Mindiola, D. J.; Caulton, K. G., A Dinuclear Cobalt Complex Featuring Unprecedented Anodic and Cathodic Redox Switches for Single-Molecule Magnet Activity. *J. Am. Chem. Soc.* **2013,** *135*, 14670-14678.
12. Doistau, B.; Benda, L.; Cantin, J.-L.; Chamoreau, L.-M.; Ruiz, E.; Marvaud, V.; Hasenknopf, B.; Vives, G., Six States Switching of Redox-Active Molecular Tweezers by Three Orthogonal Stimuli. *J. Am. Chem. Soc.* **2017,** *139*, 9213-9220.
13. Feng, X.; Mathonière, C.; Jeon, I.-R.; Rouzières, M.; Ozarowski, A.; Aubrey, M. L.; Gonzalez, M. I.; Clérac, R.; Long, J. R., Tristability in a Light-Actuated Single-Molecule Magnet. *J. Am. Chem. Soc.* **2013,** *135*, 15880-15884.
14. Sciortino, N. F.; Scherl-Gruenwald, K. R.; Chastanet, G.; Halder, G. J.; Chapman, K. W.; Létard, J.-F.; Kepert, C. J., Hysteretic Three-Step Spin Crossover in a Thermo- and Photochromic 3D Pillared Hofmann-type Metal–Organic Framework. *Angew. Chem. Int. Ed.* **2012,** *51*, 10154-10158.
15. Dapporto, P.; Dei, A.; Poneti, G.; Sorace, L., Complete direct and reverse optically induced valence tautomeric interconversion in a cobalt-dioxolene complex. *Chem. - Eur. J.* **2008,** *14*, 10915-10918.
16. Real, J. A.; Bolvin, H.; Bousseksou, A.; Dworkin, A.; Kahn, O.; Varret, F.; Zarembowitch, J., Two-step spin crossover in the new dinuclear compound $[Fe(bt)(NCS)_2]_2$bpym, with bt = 2,2'-bi-2-thiazoline and bpym = 2,2'-bipyrimidine: experimental investigation and theoretical approach. *J. Am. Chem. Soc.* **1992,** *114*, 4650-4658.
17. Verat, A. Y.; Ould-Moussa, N.; Jeanneau, E.; Le Guennic, B.; Bousseksou, A.; Borshch, S. A.; Matouzenko, G. S., Ligand Strain and the Nature of Spin Crossover in Binuclear Complexes: Two-Step Spin Crossover in a 4,4'-Bipyridine-Bridged Iron(II) Complex $[\{Fe(dpia)(NCS)_2\}_2(4,4'\text{-bpy})]$ (dpia = di(2-picolyl)amine; 4,4'-bpy = 4,4'-bipyridine). *Chem. - Eur. J.* **2009,** *15*, 10070-10082.
18. Ksenofontov, V.; Gaspar, A. B.; Niel, V.; Reiman, S.; Real, J. A.; Gütlich, P., On the Nature of the Plateau in Two-Step Dinuclear Spin-Crossover Complexes. *Chem. - Eur. J.* **2004,** *10*, 1291-1298.
19. Matouzenko, G. S.; Jeanneau, E.; Verat, A. Y.; Bousseksou, A., Spin crossover and polymorphism in a family of 1,2-bis(4-pyridyl)ethene-bridged binuclear iron(II) complexes. A key role of structural distortions. *Dalton Trans.* **2011,** *40*, 9608-9618.

20. Clements, J. E.; Airey, P. R.; Ragon, F.; Shang, V.; Kepert, C. J.; Neville, S. M., Guest-Adaptable Spin Crossover Properties in a Dinuclear Species Underpinned by Supramolecular Interactions. *Inorg. Chem.* **2018,** *57*, 14930-14938.
21. Craze, A. R.; Bhadbhade, M. M.; Kepert, C. J.; Lindoy, L. F.; Marjo, C. E.; Li, F., Solvent effects on the spin-transition in a series of Fe(II) dinuclear triple helicate compounds. *Crystals* **2018,** *8*, 376/1-376/16.
22. Cirera, J.; Ruiz, E., Theoretical modeling of two-step spin-crossover transitions in Fe^{II} dinuclear systems. *J. Mater. Chem. C* **2015,** *3*, 7954-7961.
23. Tezgerevska, T.; Alley, K. G.; Boskovic, C., Valence tautomerism in metal complexes: Stimulated and reversible intramolecular electron transfer between metal centers and organic ligands. *Coord. Chem. Rev.* **2014,** *268*, 23-40.
24. Mulyana, Y.; Poneti, G.; Moubaraki, B.; Murray, K. S.; Abrahams, B. F.; Sorace, L.; Boskovic, C., Solvation effects on the valence tautomeric transition of a cobalt complex in the solid state. *Dalton Trans.* **2010,** *39*, 4757-4767.
25. Bencini, A.; Caneschi, A.; Carbonera, C.; Dei, A.; Gatteschi, D.; Righini, R.; Sangregorio, C.; van Slageren, J., Tuning the physical properties of a metal complex by molecular techniques: the design and the synthesis of the simplest cobalt-*o*-dioxolene complex undergoing valence tautomerism. *J. Mol. Struct.* **2003,** *656*, 141-154.
26. Caneschi, A.; Dei, A.; Fabrizi de Biani, F.; Gütlich, P.; Ksenofontov, V.; Levchenko, G.; Hoefer, A.; Renz, F., Pressure- and temperature-induced valence tautomeric interconversion in a *o*-dioxolene adduct of a cobalt - tetraazamacrocycle complex. *Chem. - Eur. J.* **2001,** *7*, 3926-3930.
27. Wu, S.-Q.; Liu, M.; Gao, K.; Kanegawa, S.; Horie, Y.; Aoyama, G.; Okajima, H.; Sakamoto, A.; Baker, M. L.; Huzan, M. S.; Bencok, P.; Abe, T.; Shiota, Y.; Yoshizawa, K.; Xu, W.; Kou, H.-Z.; Sato, O., Macroscopic Polarization Change via Electron Transfer in a Valence Tautomeric Cobalt Complex. *Nat. Commun.* **2020,** *11*, 1992.
28. Poneti, G.; Poggini, L.; Mannini, M.; Cortigiani, B.; Sorace, L.; Otero, E.; Sainctavit, P.; Magnani, A.; Sessoli, R.; Dei, A., Thermal and optical control of electronic states in a single layer of switchable paramagnetic molecules. *Chem. Sci.* **2015,** *6*, 2268-2274.
29. Hearns, N. G. R.; Korcok, J. L.; Paquette, M. M.; Preuss, K. E., Dinuclear Cobalt Bis(dioxolene) Complex Exhibiting Two Sequential Thermally Induced Valence Tautomeric Transitions. *Inorg. Chem.* **2006,** *45*, 8817-8819.
30. Starikova, A. A.; Minkin, V. I., Rational design of potential spin qubits manipulated by the valence tautomerism mechanism: quantum-chemical modeling of the trinuclear transition metal complexes with bischelate linkers. *New J. Chem.* **2017,** *41*, 6497-6503.
31. Calzolari, A.; Chen, Y.; Lewis, G. F.; Dougherty, D. B.; Shultz, D.; Buongiorno Nardelli, M., Complex Materials for Molecular Spintronics Applications: Cobalt Bis(dioxolene) Valence Tautomers, from Molecules to Polymers. *J. Phys. Chem. B* **2012,** *116*, 13141-13148.
32. Poneti, G.; Mannini, M.; Cortigiani, B.; Poggini, L.; Sorace, L.; Otero, E.; Sainctavit, P.; Sessoli, R.; Dei, A., Magnetic and Spectroscopic Investigation of Thermally and Optically Driven Valence Tautomerism in Thioether-Bridged Dinuclear Cobalt-Dioxolene Complexes. *Inorg. Chem.* **2013,** *52*, 11798-11805.
33. Beni, A.; Dei, A.; Laschi, S.; Rizzitano, M.; Sorace, L., Tuning the charge distribution and photoswitchable properties of cobalt-dioxolene complexes by using molecular technique. *Chem. - Eur. J.* **2008,** *14*, 1804-1813.

34. Gransbury, G. K.; Boulon, M.-E.; Petrie, S.; Gable, R. W.; Mulder, R. J.; Sorace, L.; Stranger, R.; Boskovic, C., DFT Prediction and Experimental Investigation of Valence Tautomerism in Cobalt-Dioxolene Complexes. *Inorg. Chem.* **2019,** *58*, 4230-4243.
35. Alley, K. G.; Poneti, G.; Robinson, P. S. D.; Nafady, A.; Moubaraki, B.; Aitken, J. B.; Drew, S. C.; Ritchie, C.; Abrahams, B. F.; Hocking, R. K.; Murray, K. S.; Bond, A. M.; Harris, H. H.; Sorace, L.; Boskovic, C., Redox Activity and Two-Step Valence Tautomerism in a Family of Dinuclear Cobalt Complexes with a Spiroconjugated Bis(dioxolene) Ligand. *J. Am. Chem. Soc.* **2013,** *135*, 8304-8323.
36. Suenaga, Y.; Pierpont, C. G., Binuclear Complexes of Co(III) Containing Extended Conjugated Bis(Catecholate) Ligands. *Inorg. Chem.* **2005,** *44*, 6183-6191.
37. Nakano, K.; Kawata, S.; Yoneda, K.; Fuyuhiro, A.; Yagi, T.; Nasu, S.; Morimoto, S.; Kaizaki, S., Direct two-step spin-crossover through [HS-HS]···[LS-LS] at the plateau in dinuclear diiron(II) complex [{Fe(NCBH$_3$)(4phpy)}$_2$(μ-bpypz)$_2$]. *Chem. Commun.* **2004**, 2892-2893.
38. Alley, K. G.; Poneti, G.; Aitken, J. B.; Hocking, R. K.; Moubaraki, B.; Murray, K. S.; Abrahams, B. F.; Harris, H. H.; Sorace, L.; Boskovic, C., A Two-Step Valence Tautomeric Transition in a Dinuclear Cobalt Complex. *Inorg. Chem.* **2012,** *51*, 3944-3946.
39. Tezgerevska, T.; Rousset, E.; Gable, R. W.; Jameson, G. N. L.; Sañudo, E. C.; Starikova, A. A.; Boskovic, C., Valence tautomerism versus spin crossover in pyridinophane-cobalt-dioxolene complexes: an experimental and computational study. *Dalton Trans.* **2019,** *48*, 11674-11689.
40. Tourón Touceda, P.; Mosquera Vázquez, S.; Lima, M.; Lapini, A.; Foggi, P.; Dei, A.; Righini, R., Transient infrared spectroscopy: a new approach to investigate valence tautomerism. *Phys. Chem. Chem. Phys.* **2012,** *14*, 1038-1047.
41. Rupp, F.; Chevalier, K.; Graf, M.; Schmitz, M.; Kelm, H.; Grün, A.; Zimmer, M.; Gerhards, M.; van Wüllen, C.; Krüger, H.-J.; Diller, R., Spectroscopic, Structural, and Kinetic Investigation of the Ultrafast Spin Crossover in an Unusual Cobalt(II) Semiquinonate Radical Complex. *Chem. - Eur. J.* **2017,** *23*, 2119-2132.
42. Halcrow, M. A., Structure:function relationships in molecular spin-crossover complexes. *Chem. Soc. Rev.* **2011,** *40*, 4119-4142.
43. Ketkaew, R.; Tantirungrotechai, Y.; Harding, D. J.; Harding, P.; Marchivie, M. *OctaDist version 2.4*, 2019.
44. Llunell, M.; Casanova, D.; Cirera, J.; Alemany, P.; Alvarez, S. *SHAPE*, 2.1; Universitat de Barcelona: Barecelona, Spain, 2013.
45. Alvarez, S.; Avnir, D.; Llunell, M.; Pinsky, M., Continuous symmetry maps and shape classification. The case of six-coordinated metal compounds. *New J. Chem.* **2002,** *26*, 996-1009.
46. Gransbury, G. K.; Boulon, M.-E.; Gable, R. W.; Mole, R. A.; Moubaraki, B.; Murray, K. S.; Sorace, L.; Soncini, A.; Boskovic, C., Single ion anisotropy and exchange coupling in cobalt(II)-radical complexes: insights from magnetic and ab initio studies. *Chem. Sci.* **2019,** *10*, 8855-8871.
47. Carugo, O.; Castellani, C. B.; Djinović, K.; Rizzi, M., Ligands derived from o-benzoquinone: statistical correlation between oxidation state and structural features. *J. Chem. Soc., Dalton Trans.* **1992**, 837-841.
48. Brown, S. N., Metrical Oxidation States of 2-Amidophenoxide and Catecholate Ligands: Structural Signatures of Metal-Ligand π Bonding in Potentially Noninnocent Ligands. *Inorg. Chem.* **2012,** *51*, 1251-1260.

49. Kahn, O., *Molecular Magnetism*. VCH Publishers, Inc.: New York, NY, 1993.
50. Panja, A.; Jana, N. C.; Bauzá, A.; Frontera, A.; Mathonière, C., Solvent-Triggered Cis/Trans Isomerism in Cobalt Dioxolene Chemistry: Distinguishing Effects of Packing on Valence Tautomerism. *Inorg. Chem.* **2016,** *55*, 8331-8340.
51. Yu, F.; Xiang, M.; Wu, Q.-g.; He, H.; Cheng, S.-q.; Cai, X.-y.; Li, A.-h.; Zhang, Y.-m.; Li, B., Valence tautomerism and photodynamics observed in a dinuclear cobalt-tetraoxolene compound. *Inorg. Chim. Acta* **2015,** *426*, 146-149.
52. Caneschi, A.; Dei, A.; Gatteschi, D.; Tangoulis, V., Antiferromagnetic Coupling in a Six-Coordinate High Spin Cobalt(II)-Semiquinonato Complex. *Inorg. Chem.* **2002,** *41*, 3508-3512.
53. Bencini, A.; Beni, A.; Costantino, F.; Dei, A.; Gatteschi, D.; Sorace, L., The influence of ligand field effects on the magnetic exchange of high-spin Co(II)-semiquinonate complexes. *Dalton Trans.* **2006**, 722-729.
54. Chen, X.-Y.; Wei, R.-J.; Zheng, L.-S.; Tao, J., Valence Tautomeric Transitions of Three One-Dimensional Cobalt Complexes. *Inorg. Chem.* **2014,** *53*, 13212-13219.
55. da Silva, A. F. M.; de Mello, M. V. P.; Gómez, J. G.; Ferreira, G. B.; Lanznaster, M., Investigation of cobalt(III)-tetrachlorocatechol complexes as models for catechol-based anticancer prodrugs. *Eur. J. Inorg. Chem.* **2019**, 1784-1791.
56. Demadis, K. D.; Hartshorn, C. M.; Meyer, T. J., The Localized-to-Delocalized Transition in Mixed-Valence Chemistry. *Chem. Rev.* **2001,** *101*, 2655-2686.
57. D'Alessandro, D. M.; Keene, F. R., Current trends and future challenges in the experimental, theoretical and computational analysis of intervalence charge transfer (IVCT) transitions. *Chem. Soc. Rev.* **2006,** *35*, 424-440.
58. Brunschwig, B. S.; Sutin, N., Energy surfaces, reorganization energies, and coupling elements in electron transfer. *Coord. Chem. Rev.* **1999,** *187*, 233-254.
59. D'Alessandro, D. M.; Topley, A. C.; Davies, M. S.; Keene, F. R., Probing the Transition between the Localised (Class II) and Localised-to-Delocalised (Class II–III) Regimes by Using Intervalence Charge-Transfer Solvatochromism in a Series of Mixed-Valence Dinuclear Ruthenium Complexes. *Chem. – Eur. J.* **2006,** *12*, 4873-4884.
60. Poddel'sky, A. I.; Smolyaninov, I. V.; Vavilina, N. N.; Kurskii, Y. A.; Berberova, N. T.; Cherkasov, V. K.; Abakumov, G. A., Triaryl- and trialkylantimony(V) Bis(catecholates) based on 1,1'-Spirobis[3,3-dimethylindanequinone-5,6]: Spectroscopic and electrochemical studies. *Russ. J. Coord. Chem.* **2012,** *38*, 284-294.
61. Dei, A.; Gatteschi, D.; Sangregorio, C.; Sorace, L., Quinonoid Metal Complexes: Toward Molecular Switches. *Acc. Chem. Res.* **2004,** *37*, 827-835.
62. Dei, A.; Sorace, L., pH-Triggered intramolecular electron transfer in asymmetric bis-dioxolene adducts. *Dalton Trans.* **2003**, 3382-3386.
63. Loughrey, J. J.; Sproules, S.; McInnes, E. J. L.; Hardie, M. J.; Halcrow, M. A., Stable Mixed-Valent Radicals from Platinum(II) Complexes of a Bis(dioxolene) Ligand. *Chem. - Eur. J.* **2014,** *20*, 6272-6276.
64. Tahara, K.; Kadowaki, T.; Kikuchi, J.-i.; Ozawa, Y.; Yoshimoto, S.; Abe, M., Synthesis and Characterization of a New Series of Binuclear Pd(II) Biscatecholato Complexes: Non-Innocent Ligand-Based Approach to a Wide Range of Variation in Near-Infrared Absorptions of Mixed-Valence Complexes. *Bull. Chem. Soc. Jpn.* **2018,** *91*, 1630-1639.

65. Hildebrandt, A.; Miesel, D.; Yuan, Q.; Freytag, J.; Mahrholdt, J.; Lang, H., Anion and solvent dependency of the electronic coupling strength in mixed valent class II systems. *Dalton Trans.* **2019,** *48*, 13162-13168.
66. Minkin, V. I.; Starikov, A. G.; Starikova, A. A., Computational insight into magnetic behavior and properties of the transition metal complexes with redox-active ligands: a DFT approach. *Pure Appl. Chem.* **2018,** *90*, 811-824.
67. Sato, D.; Shiota, Y.; Juhász, G.; Yoshizawa, K., Theoretical Study of the Mechanism of Valence Tautomerism in Cobalt Complexes. *J. Phys. Chem. A* **2010,** *114*, 12928-12935.
68. Adams, D. M.; Noodleman, L.; Hendrickson, D. N., Density Functional Study of the Valence-Tautomeric Interconversion Low-Spin $[Co^{III}(SQ)(Cat)(phen)]$ ⇌ High-Spin $[Co^{II}(SQ)_2(phen)]$. *Inorg. Chem.* **1997,** *36*, 3966-3984.
69. Minkin, V. I.; Starikov, A.; Starikova, A. A., Theoretical Modeling of Valence Tautomeric Dinuclear Cobalt Complexes. Adducts of Co^{II} Diketonates with Cyclic Redox-Active Tetraone Ligands. *Dalton Trans.* **2015,** *44*, 17819-17828.
70. Minkin, V. I.; Starikova, A. A.; Starikov, A. G., Valence tautomeric dinuclear adducts of Co(II) diketonates with redox-active diquinones for the design of spin qubits: computational modeling. *Dalton Trans.* **2015,** *44*, 1982-1991.
71. Starikova, A. A.; Starikov, A. G.; Minkin, V. I., Valence-tautomeric adducts of Co(II) diketonates based on annelated di-o-quinones: Computer simulation. *Russ. J. Coord. Chem.* **2017,** *43*, 197-205.
72. Zein, S.; Borshch, S. A., Energetics of Binuclear Spin Transition Complexes. *J. Am. Chem. Soc.* **2005,** *127*, 16197-16201.
73. Noodleman, L., Valence bond description of antiferromagnetic coupling in transition metal dimers. *J. Chem. Phys.* **1981,** *74*, 5737-5743.
74. Starikova, A. A.; Chegerev, M. G.; Starikov, A. G.; Minkin, V. I., A DFT computational study of the magnetic behaviour of cobalt dioxolene complexes of tetraazamacrocyclic ligands. *Comput. Theor. Chem.* **2018,** *1124*, 15-22.

FOR TABLE OF CONTENTS ONLY